PHYTOCHROME INTERACTING FACTOR 7 moderates the activity and the cytosolic-nuclear shuttling of PHYTOCHROME A

Mengke Zhou[1*], Andrés Romanowski[2], Karen J. Halliday[1*]

1. Institute for Molecular Plant Sciences, School of Biological Sciences, University of Edinburgh, Edinburgh EH9 3BF, United Kingdom.

2. Timing of Environmental Signaling lab, Molecular Biology Group, Plant Sciences, Wageningen University & Research, Wageningen, The Netherlands.

ORCID IDs: 0000-0003-1043-2766 (MK. Z); 0000-0003-0737-2408 (A.R.); 0000-0003-0467-104X (K.J.H.).

*Corresponding authors:
Mengke Zhou and Karen J. Halliday
Institute for Molecular Plant Sciences, School of Biological Sciences, University of Edinburgh, Edinburgh EH9 3BF, United Kingdom
+44-0131-651-9083
mengke.zhou@ed.ac.uk
karen.halliday@ed.ac.uk

ABSTRACT

In nature, plants sense and navigate complex vegetative environments using the phytochrome (phy) photoreceptor-signaling system. The canopy adaptation strategy, elicited by phyA, and the shade avoidance syndrome, regulated by phyB, allow plants to adapt to diverse forms of vegetation shade. The phyA High Irradiance Response (HIR) mode, involving photocycle-coupled nuclear shuttling, is essential for detecting persistent far-red rich conditions typical of canopy or occlusive shade. Our research identifies PHYTOCHROME INTERACTION FACTOR 7 (PIF7) as a critical regulator of phyA function. We demonstrate PIF7ox can effectively block phyA action. In persistent shade, PIF7 and phyA both accumulate and interact within nuclear bodies, with binding facilitated through the prion-like domain of PIF7 and the C-terminal PAS-PAS domain of phyA. PIF7 also interacts with FHY1 and FHL chaperones, interfering with phyA cytosolic-nuclear shuttling. This strategic molecular targeting by PIF7 provides an effective strategy for modulating the phyA HIR in response to shade signals.

INTRODUCTION

Light sensing is fundamental for plant adaptation and survival in vegetative shade. This is particularly important during seedling establishment, a stage when plants are most vulnerable. Plants have evolved distinct developmental strategies to cope with different types of shade that are prevalent in nature. The light receptor phytochrome B (phyB), is able to detect FR-rich light from neighboring plants and elicit the Shade Avoidance Syndrome (SAS), which induces elongation of seedling hypocotyls, repositions leaves to improve light capture, and triggers early flowering[1,2]. Under persistent canopy shade, plants adopt alternative strategies, such as the phyA-mediated Canopy Adaptation Strategy (CAS), which suppresses hypocotyl elongation and conserves resources, optimizing growth when shade is unyielding[3]. As vegetative habitats can change considerably through a season, the ability to adjust photoreceptor activity offers adaptive flexibility, ensuring successful seedling establishment and progression through the life cycle.

In Arabidopsis, phytochromes A-E, form a family of photoreceptors that principally absorb light in the red (R) and far-red (FR) regions of the spectrum[4]. Absorption of R photoconverts phytochrome into its active Pfr form, while FR photoconverts Pfr to the inactive Pr conformer.

When activated phytochromes move from the cytosol to the nucleus where they aggregate in sub-nuclear photobodies to perform a range of functions[5,6]. While all phytochromes possess similar photosensory properties, they fall into two classes based on their distinct modes of action. Phytochromes B-E, which operate in the low fluence response (LFR) mode, are activated by R and deactivated by FR light. Consequently, in FR-rich vegetation shade environments, these phytochromes are less active[4,7]. A key distinction of phyA is that it is activated by FR-rich light through its high irradiance response (HIR) mode of action[7]. This property arises partly from its photobiology and partly from the shuttling mechanism that concentrates phyA in the nucleus[8]. PhyA lacks a nuclear localization signal and primarily relies on the chaperone proteins FHY1/FHL to facilitate its transport into the nucleus. These proteins specifically recognize phyA-Pfr and transport it to the nucleus, where it is converted into phyA-Pr, allowing FHY1/FHL to dissociate and be recycled to the cytoplasm for further shuttling[8,9,10]. Nuclear located phyA regulates a number of processes, including expression of target genes, through association with transcription factors such as PHYTOCHROME INTERACTING FACTORS (PIFS) and ELONGATED HYPOCOTYL 5 (HY5)[11]. The central role of FHY1/FHL shuttling in the phyA HIR, identifies this mechanism as a potential target for modifying phyA action and the adaptive response[8]. Indeed, HY5 has been reported to be involved in negative-feedback regulation of phyA signaling through repressing FHY1/FHL expression[11]. Here, HY5 directly interacts with the DNA-binding regions of FAR-RED ELONGATED HYPOCOTYLS 3 (FHY3) and FAR-RED IMPAIRED RESPONSE 1 (FAR1) to prevent their transcriptional activation of FHY1/FHL.

PIF transcription factors are well-studied negative regulators of phytochrome signaling. They function by directly binding to G/PBE-boxes in the promoters of their target genes[12]. In Arabidopsis, there are eight PIFs (PIF1, PIF2/PIL1-PIF8), each with an active phytochrome B (APB) domain that facilitates their interaction with phyB. Only PIF1 and PIF3 contain an active phytochrome A (APA) domain, which directly binds the C-terminus of phyA, comprising two Period-Arnt-SIM (PAS) and a histidine kinase-related (HKRD) domains[13]. In FR light, phyA directly interacts with PIF1 and PIF3, triggering their proteolytic destruction and/or sequestration from target promoters[13,14]. Although PIF4, PIF5, PIF8 and PIF7 lack an APA

domain, they have been shown to control aspects of phyA signaling[15,16,17]. Interestingly, levels of PIF8 protein are boosted by phyA. In darkness, CONSTITUTIVE PHOTOMORPHOGENESIS 1 (COP1) promotes PIF8 protein degradation through the 26S proteasome, thereby reducing its abundance. Conversely, under FR light, phyA inhibition of COP1 stabilizes the PIF8 protein, forming a negative feedback loop that limits phyA action[15].

Notably, PIF7, a close homologue of PIF8, is a potent regulator of SAS. In unshaded conditions, PIF7 interacts with active phyB (Pfr) through its APB domain, and both proteins localize to sub-nuclear photobodies. This interaction prevents PIF7 from binding to the promoters of target genes, effectively inhibiting PIF7-regulated gene expression[18,19]. Under shade conditions, the deactivation of phyB releases PIF7 from this repression, leading to the activation of shade-responsive genes and triggering the physiological SAS response[20,21]. Furthermore, exposure to shade triggers the dephosphorylation and nuclear accumulation of PIF7, processes that enhance the activation of SAS[20]. Given its strong promotory role in SAS, it is notable that PIF7 has recently been demonstrated to increase *PHYA* transcript abundance, an action that could potentially limit SAS. This PIF7 action can be inhibited by *PHYA UTR ANTISENSE RNA (PUAR),* which binds to PIF7 and prevents its interaction with *PHYA's* 5' UTR, thereby reducing *PHYA* transcript levels[17]. Collectively, this research underscores the importance of PIF7 as a key agent in executing and moderating the molecular response to shade.

Here, we show that PIF7 modulates phyA signaling under vegetative shade by controlling phyA subcellular localization and activity. PIF7 overexpression (PIF7ox) abolishes phyA-mediated suppression of seedling hypocotyl elongation under persistent shade. Under these conditions, PIF7 and phyA co-localize in nuclear photobodies and interact directly via the PIF7 prion-like domain and the phyA C-terminus. Additionally, our data shows that PIF7 governs phyA subcellular localization by modulating FHY1/FHL-dependent nuclear import. These insights clarify how PIF7 effectively restricts both the nuclear transport and signaling activities of phyA, illuminating the intricate molecular mechanisms at play.

RESULTS

105 **PIF7ox blocks phyA action**

106 PIF7, which functions downstream of phyB, also shares significant sequence similarity with
107 PIF8, a regulator of phyA responses. This similarity led us to investigate the potential genetic
108 interaction between PIF7 and phyA. To achieve this, we measured the hypocotyl length of
109 seedlings grown under two conditions: 8h white light (WL): 16h dark (D), and 8h low R:FR
110 ratio (0.2) light (WLFR). Both photoperiods started one day after germination to strongly elicit
111 a phyA response (Fig. 1a). As expected, wild type (WT, Col-0) seedlings were slightly shorter
112 in WLFR compared to WL, while *phyA-211* had longer hypocotyls in WLFR due to reduced
113 control of shade-avoidance elongation (Fig. 1b-c). In contrast, the phyAox line displayed a
114 constitutively short hypocotyl and retained WLFR-responsivity. In WL, the *pif7-1, pif7-2* loss-
115 of-function alleles were marginally shorter than the WT but retained a response to WLFR that
116 was absent in the *pif7-1*; *phyA-211* double mutant. In keeping with PIF7's function in promoting
117 the phyB-mediated shade response, under WLFR, *pif7-1* diminishes the impact of *phyA-211* on
118 hypocotyl length. Conversely, hypocotyls of *p35S::PIF7-FLASH* (PIF7ox) seedlings were
119 elongated in WL and exhibited further elongation under WLFR. As hypocotyl lengths were
120 similar in PIF7ox and PIF7ox;*phyA-211,* this suggests PIF7ox facilitates increased shade-
121 avoidance elongation while simultaneously suppressing phyA action (Fig. 1c)[18]. This
122 observation infers that PIF7 may participate in phyB to phyA cross-regulation.

123 Given the capacity of PIF7ox to inhibit phyA activity, we sought to investigate the possibility
124 of functional redundancy with other PIFs. As anticipated, PIF8ox also lacked WLFR-mediated
125 growth inhibition, but PIF3ox, PIF4ox and PIF5ox all retained this response (Fig. S1a-b)[15]. Our
126 data therefore illustrate that even though PIF3, PIF4 and PIF5 have been implicated in *PHYA*
127 regulation and signaling, their functions diverge from PIF7 and PIF8[16,22,23]. We found the
128 hypocotyl lengths of *pif8-1* and *pif8-1;phyA-211* were qualitatively similar to *pif7-1, pif7-2*, and
129 *pif7-1;phyA-211*, respectively (Fig. S1c). However, comparison of the *PIF7ox;phyA-211* and
130 *PIF8ox;phyA-211* lines reveals distinct differences in PIF7 and PIF8. While PIF7ox is epistatic
131 to *phyA-211*, this genetic relationship shifts for PIF8, particularly under WLFR, where we show
132 *phyA-211* is epistatic to PIF8ox. This finding aligns well with evidence showing PIF8 functions

133 downstream of phyA[15].

134 These results show PIF7 has a distinct role in antagonizing the suppression of hypocotyl growth
135 by phyA, a phenomenon particularly evident in the PIF7ox lines, which effectively block this
136 response.

137 **PIF7 moderates phyA protein abundance**

138 PIF7 is known to promote shade induction of *PHYA* expression by binding to its 5' UTR[17].
139 Concurring with this study, we found that when sampled one hour before dusk (ZT7) in an
140 8L:16D photoperiod, WLFR enhanced *PHYA* gene expression in the WT, whereas this response
141 was diminished in the *pif7-1* mutant. Likewise, PIF7ox exhibited elevated *PHYA* levels in
142 control conditions, which were further enhanced in WLFR (Fig. 1d). Immunoblot analysis
143 using an antibody against native phyA, reported phyA levels to be consistently low in WL,
144 across all genotypes. We observed that WLFR led to an increase in phyA protein levels in WT,
145 *pif7-1* and PIF7ox, which qualitatively corresponded with the patterns seen in *PHYA* mRNA
146 data (Fig. 1d-f). Further, we found that PIF7ox had a negligible effect on the *pPHYA::PHYA-*
147 *nLUC* (phyA-nLUC) in WL, which is known to gradually deplete under these conditions. In-
148 line previous studies, we observed higher levels of daytime phyA-nLUC in WLFR, which was
149 notably elevated by PIF7ox (Fig. 1g)[3]. Collectively, these findings demonstrate that under
150 WLFR conditions, PIF7 regulates *PHYA* expression and the abundance of phyA protein.
151 Interestingly, despite PIF7ox accumulating significantly higher levels of phyA under WLFR,
152 PIF7ox seedlings fail to elicit a phyA response. This indicates that the regulatory effect of PIF7
153 on phyA activity does not stem from changes in phyA abundance.

154 To examine the *in vivo* dynamics of PIF7 under our experimental conditions, we generated
155 *pPIF7::PIF7-nLUC* (PIF7-nLUC) lines. We discovered that PIF7-nLUC exhibits rhythmic
156 patterns, with higher levels during the day compared to the night (Fig. S2a). WLFR boosted
157 daytime levels of PIF7-nLUC levels, with the *phyA-211* mutation elevating PIF7-nLUC toward
158 the end of the period, especially in WLFR (Fig. S2b). Therefore, our data indicated that similar
159 to phyA, WLFR increases the abundance of PIF7, and that phyA plays a minor role in reducing

160 PIF7 production toward the end of the photoperiod.

161 **PIF7 can interact with phyA in nuclear photobodies**

162 To establish whether PIF7 and phyA interact *in planta* we first used *p35S::PIF7-sfGFP* (PIF7-
163 GFP) and *p35S::PHYA-RFP* (phyA-RFP) transiently expressed in *N. benthamiana* leaves to
164 establish whether PIF7 are found in the same cellular location. We found that following WLFR
165 treatment PIF7-GFP and phyA-RFP co-localize in nuclei and in sub-nuclear foci, or
166 photobodies (Fig. 2a). Quantitative fluorescence measurements along a nuclear transect,
167 intersecting two photobodies, clearly show this co-localization (Fig. 2a). Next, we created split
168 bimolecular fluorescence complementation (BiFC) constructs *p35S::PIF7-nYFP* (PIF7-nYFP)
169 and *p35S::PHYA-cYFP* (phyA-cYFP*)*, to test whether PIF7 and phyA physically interact *in vivo*.
170 In WLFR, BiFC assays yielded strong nuclear and sub-nuclear foci signals, but not in control
171 lines expressing *p35S::PIF7-nYFP* and *p35S::EV-cYFP.* The data suggest PIF7 and phyA are
172 indeed able to interact in nuclei and within photobodies under WLFR (Fig. 2b).

173 To gain further evidence for this interaction we also generated split nanoLUC (nLUC) luciferase
174 reporter constructs, *p35S::PIF7-lgbitnLUC* (PIF7-lgbit) and *p35S::PHYA-smbitnLUC* (phyA-
175 smbit), with *p35S::PHYB-smbitnLUC* (phyB-smbit) and *p35S::PHYA-nLUC* (phyA-nLUC) as
176 controls (Fig. 2c). As expected, we found a strong signal in the PIF7-lgbit+phyB-smbit in WL
177 which is diminished in WLFR, which is consistent with the known light conditional interaction
178 between PIF7 and phyB[18]. Again, as expected we observed a strong signal from phyA-nLUC
179 in WLFR, which is known to increase phyA abundance, while negative controls (phyA-smbit+
180 phyB-smbit) had low signal in both conditions. In WL conditions, the signal from PIF7-lgbit +
181 phyA-smbit was low, similar to that of the negative control, whereas in WLFR conditions, the
182 signal was strong, indicating an interaction. Further, using an antibody to native phyA we
183 demonstrated co-immunoprecipitation of phyA with PIF7ox, in WLFR but not WL conditions
184 (Fig. 2d). Thus, our data provides evidence that PIF7 and phyA directly interact within
185 photobodies after exposure to WLFR, which promotes their respective nuclear
186 accumulation[20,24].

187 **Prion-like Domain of PIF7 interacts with phyA PAS-PAS Domain**

188 Earlier work demonstrated that phyA binds directly with PIF1 and PIF3. The phyA C-terminal
189 output module (OPM) is known to be important for this interaction, as is the active phyA-
190 binding domains (APA) of PIF1 and PIF3[13,22]. To identify PHYA regions that required for the
191 molecular interaction we utilized *p35S::PIF7-nYFP* (PIF7-nYFP) and *p35S::PHYA-cYFP*
192 (phyA-cYFP) split YFP assay, creating truncated PHYA constructs as follows: C-terminal
193 (PHYA-C), comprising HINGE (H), PAS-PAS DOMAIN (PAS), and HISTIDINE KINASE
194 RELATED DOMAIN (HKRD) regions [*H+PAS+HKRD-cYFP*], PHYA-C1 [*PAS+HKRD-*
195 *cYFP*], PHYA-P [*PAS-cYFP*], and PHYA-H [*HKRD-cYFP*] (Fig. 3a). In WLFR we obtained
196 nuclear fluorescence signals for PIF7-nYFP and the full-length phyA-cYFP control, as well as
197 the truncated PHYA-C, PHYA-C1, and PHYA-P constructs. No signal was observed for PHYA-
198 H and the negative EV control. The strong signal detected for PHYA-P, which includes PAS-
199 PAS domain motifs, highlights the significance of this molecular region in facilitating the
200 interaction with PIF7. To identify the region of PIF7 that mediated the interaction with phyA,
201 we generated PIF7-N which contains the ACTIVE PHYTOCHROME BINDING domain
202 [*PIF7-N-nYFP*], PIF7-B, containing the BASIC HELIX-LOOP-HELIX motif [*PIF7-B-nYFP*],
203 and PIF7-C which contains a Prion-like domain (PrLD) [*PIF7-C-nYFP*] which has a polyQ-
204 rich sequence is located at PrLD center (Fig. 3b, Fig. S6). Interestingly we found that only the
205 PIF7 full length control and PIF7-C gave nuclear fluorescence in WLFR. Thus, our data point
206 to the prion-like domain of PIF7 as being important for its interaction with phyA. Since PIF7
207 lacks an APA domain, it seems that prion region is able to fulfill this role.

208 **PIF7 regulates the subcellular localization of phyA**

209 Our data show PIF7ox elevates phyA protein levels, yet PIF7ox lines are unable to mount a
210 phyA response in WLFR conditions. Given that WLFR stimulates the phyA HIR and its nuclear
211 accumulation, we sought to analyze the subcellular localization more closely. As anticipated,
212 confocal microscopy revealed strong cytosolic and weaker nuclear signals for phyA-GFP
213 (*pPHYA::PHYA-sGFP*), and for GFP-PIF7 (*p35S::GFP-PIF7*) when in WL (Fig. S3). Exposure
214 to WLFR notably enhanced nuclear relative to cytosolic signals, confirming the nuclear

215 accumulation of both PIF7 and phyA under our shade conditions (Fig. S3a)[19,20,25]. We then
216 aimed to establish if PIF7 affected the subcellular localization of phyA by introgressing phyA-
217 GFP into *pif7-1* and PIF7ox backgrounds. In WL, we found phyA-GFP to be predominantly in
218 the cytosol in *Col-0*, *pif7-1* and PIF7ox lines (Fig. 4a). Under WLFR, we recorded a higher
219 proportion of nuclear phyA-GFP in WT, with an even greater increase in the *pif7-1* mutant,
220 whereas significantly lower levels were detected in PIF7ox (Fig. 4b-c). Thus, PIF7 appears to
221 influence the cytoplasmic to nuclear partitioning of phyA-GFP. To verify our results, we
222 performed immunoblot assays that differentiated between nuclear and cytosolic fractions. This
223 method yielded qualitatively similar results showing increased nuclear phyA in *pif7-1* and
224 predominately cytosolic PHYA in PIF7ox (Fig. 4d-e). Thus, our findings indicate that PIF7
225 modifies subcellular phyA localization. The notably reduced nuclear presence of phyA in
226 PIF7ox could partially account for the disrupted phyA signaling observed in PIF7ox.

227 **PIF7ox blocks phyA regulation of target genes**

228 To further interrogate the mechanism through which PIF7 inhibits phyA action we initially
229 tested whether PIF7 alters the expression of genes (*CHS, BIN2, FHY3, FHY1*, *FHL* and *IAA29)*
230 known to be directly regulated by phyA (Fig. 5a)[26,27]. As determined by qPCR all the genes,
231 except *IAA29*, were upregulated in WT in WLFR conditions, otherwise, the expression patterns
232 fell into two categories. In WLFR conditions, *CHS, BIN2,* and *FHY3* exhibited decreased
233 expression in both *phyA-211* and PIF7ox, while their expression was increased in *pif7-1*. This
234 gene set is upregulated by phyA in WLFR, and their expression is repressed by PIF7. On the
235 other hand, *FHY1, FHYL* and *IAA29* form a group that are upregulated in *phyA-211* and PIF7ox,
236 and for *FHY1* and *FHYL*, expression is lowered in *pif7-1*. These genes are downregulated by
237 phyA in WLFR, and their expression is promoted by PIF7. The common factor for all these
238 genes is that phyA and PIF7 exert opposing control of their regulation, particularly in WLFR.
239 We then sought to establish if the antagonistic action of PIF7 was mediated through direct
240 repression of phyA at target gene promoters. Here we performed chromatin
241 immunoprecipitation (ChIP) using a native phyA antibody, and qPCR using to detect phyA
242 enrichment at *CHS, FHY1*, and *FHL* promoters (Fig. 5b). For all three genes we found WLFR

243 stimulated phyA enrichment at promoter regions sequences containing G-box motifs (two in
244 CHS), but not in G-box-free regions (Control, coding region). This enrichment was eliminated
245 in the presence of PIF7ox, suggesting the interaction between PIF7 and phyA is able to block
246 phyA regulation of target genes.

247 **PIF7 interacts with FHY1 and FHL**

248 In WLFR phyA cytosolic to nuclear shuttling is controlled by FHY1 and FHL chaperones[9]. The
249 central importance of this mechanism for phyA function is evident in the *fhy1-3;fhl-1* double
250 mutant hypocotyl response which is phenotypically similar to *phyA-211* (Fig. S4). An intriguing
251 finding of our study is that PIF7 appears to control the subcellular localization of phyA. We
252 therefore wanted to establish if this arose through a process involving PIF7 interaction with
253 FHY1 and FHL. Using the *N. benthamiana* transient expression system, we recorded nuclear
254 interactions between the BiFC constructs *p35S::FHY1-cYFP*, *p35S::FHL-cYFP*, and
255 *p35S::PIF7-nYFP* under WLFR conditions (Fig. 6a). We also observed PIF7 interactions with
256 FHY1 and FHL, but not the negative control using a split nLUC assay (Fig. 6b). It is worth
257 noting that in this assay the interaction signal strength between the shuttle proteins and PIF7
258 was lower than that between PIF7 and phyA (Fg. 6b). However, we were able to verify these
259 interactions through co-immunoprecipitation using *p35S::FHY1/FHL-nLUC* (FHY1/FHL-
260 nLUC) and *p35S::PIF7-sfGFP* (PIF7-GFP) (Fig. 6c). As our data shows that PIF7 can interact
261 with phyA, FHY1 and FHL, we postulated that these proteins may form a complex under
262 inductive WLFR conditions. Supporting this hypothesis, we found that when FHY1-YFP or
263 FHL-YFP are co-expressed with PIF7-GFP and phyA-RFP in *N. benthamiana* leaves, these
264 constructs localize to the same nuclear regions under WLFR (Fig. 6d-e).

265 We also observed increased levels of *ARABIDOPSIS SUMO PROTEASE 1 (ASP1)*, a crucial
266 factor in SUMOylation and the maintenance of FHY1 levels under FR light conditions[28], in
267 PIF7ox compared to WT in WL. In WT, *ASP1* levels are increased by WLFR, a response that
268 is further amplified by *pif7-1* and suppressed by PIF7ox (Fig. 6f). Thus, PIF7 regulation of
269 *ASP1* may play a role in its control of the shuttling mechanism.

To determine if PIF7 primarily acts by sequestering phyA or whether the PIF7 interactions with FHY1/FHL are also important, we employed *pPHYA::PHYA-sGFP-NLS* (phyA-NLS), where phyA is constitutively nuclear (Fig. S7)[29]. In line with earlier findings, under our experimental conditions, phyA-NLS restores the *phyA-201* elongated hypocotyl phenotype to WT length (Fig. 6g). We hypothesized that if PIF7 regulation of phyA was solely due to its sequestration of phyA, then PIF7ox should diminish the function of phyA-NLS through this mechanism[29]. However, our data show phyA-NLS exhibits strong epistasis over PIF7ox, for hypocotyl length, and the expression of *CHS* and *IAA29* under WLFR (Fig. 6g, S5). Consequently, it seems that the mechanism of phyA sequestration alone likely cannot explain the potent effects of PIF7ox on phyA action. Previous research demonstrated that phyA-NLS completely restores phyA control of hypocotyl growth in *fhy1-3;fhl-1 and phyA-211;fhy1-3;fhl-1*, indicating that phyA-NLS can bypass the requirement for nuclear shuttling[30]. Consequently, our results imply that the interaction between PIF7 and FHY1/FHL may be required to suppress phyA action. Under WLFR, the transport of phyA into the nucleus is highly dynamic. Therefore, PIF7 may interact with phyA-FHY1/FHL complexes soon after their nuclear entry and before the complexes disassemble. This scenario is consistent with our co-localization data (Fig. 6d)[9]. Collectively, our data indicates that PIF7 forms inactive complexes with phyA and FHY1/FHL, which simultaneously impedes phyA shuttling and signaling.

DISCUSSION

The operating properties of phyA are distinct from other phytochromes. Under shaded conditions, phyA requires a cytosolic to nuclear shuttling mechanism to operate effectively, a process facilitated by the chaperone proteins FHY1 and FHL. In this study, we have shown PIF7 is a potent regulator of this process, limiting the availability of phyA for signaling. The impact on phyA is most extreme in the PIF7ox line, where WLFR-induced phyA action is blocked. Our research illustrates that PIF7 moderates phyA intracellular movement and signaling through molecular sequestration.

Studies have shown that both PIF7 and phyA accumulate in the nucleus under FR-rich shade conditions[31,18,29]. Our findings further reveal that PIF7-GFP and phyA-RFP co-localise to

298 specific sub-nuclear foci, where they physically interact as evidenced by BiFC (Fig. 2a-b).
299 Additional confirmation of this interaction was provided by split nLUC assays employing PIF7-
300 lgbit and phyA-smbit, along with co-immunoprecipitation of PIF7ox and phyA.

301 While all PIFs have an active phytochrome B (APB) domain that enables binding to phyB, only
302 PIF1 and PIF3 have active phytochrome A (APA) motifs, through which they interact with the
303 phyA C-terminus[15,32]. This binding is known to facilitate the proteolysis of PIF1 and PIF3, and
304 to inhibit the activity of PIF3 by isolating it from target promoters[15,32,33]. Our research has
305 demonstrated that although PIF7 lacks an APA domain, it can still directly interact with phyA.
306 This binding is facilitated through the PAS domain of phyA and the C-terminal region of PIF7,
307 which contains a prion-like domain. PIF7 moderates the activity of phyA by inhibiting its ability
308 to bind to target promoters (Fig. 5b). For the genes *CHS*, *FHY3*, and *BIN2*, which are activated
309 by phyA in WLFR, and for *FHY1*, *FHL*, *IAA29*, which are repressed by phyA, PIF7 counteracts
310 the effects of phyA.

311 PIF7 is particularly effective in FR-rich shade, which triggers its dephosphorylation, increases
312 its abundance, and enhances its accumulation in nuclear photobodies (Fig. S3b)[20]. Shade also
313 deactivates phyB, which typically limits the DNA-binding capacity of PIF7[19]. Since continuous
314 shade also stimulates phyA activity, it creates conducive conditions for the interaction between
315 PIF7 and phyA.

316 We have demonstrated that PIF7 and phyA interact within sub-nuclear structures known as
317 photobodies[5]. These photobodies are essentially molecular condensates that form through
318 liquid-liquid phase separation (LLPS), accompanied by a nucleation step. Nucleation aids
319 sequestration, particularly at low concentrations, and targets the formation of photobodies to
320 specific sub-nuclear sites[6,34]. Across organisms, the spatial organization of biomolecules into
321 distinct cellular locations is essential for enabling specialized functions[35].

322 PIF7 is unique amongst PIF proteins as it contains a prion-like domain with a central polyQ
323 stretch of 17 consecutive glutamine residues. PIF8 is the closest in sequence similarity to PIF7,
324 and while does possess a short polyQ sequence in its C-terminus, this domain exhibits low
325 prion-like predictability (Fig. S6). Prion-like domains (PrLD) typically comprise low-

326 complexity or intrinsically disordered regions that facilitate protein condensation and LLPS.
327 Indeed, PIF7 is able to form condensates with LLPS characteristics *in vitro*, which is proposed
328 to facilitate the formation of PIF7-phyB photobodies[19]. Substituting polyQ with polyA
329 diminishes the capacity of PIF7 to form photobodies, highlighting the importance of polyQ in
330 this process. Interestingly, phyB has also been shown to possess LLPS characteristics, for its
331 C-terminus, and disordered N-terminal extension have both been shown to phase-separate in
332 mammalian cells[36]. We have shown that in WLFR, PIF7 interacts with the phyA, through its
333 PrLD, which results in the formation of PIF7-phyA-containing photobodies. Within these
334 biomolecular condensates, phyA-mediated signaling and control of hypocotyl growth are
335 suppressed. In the PIF7ox line, this inhibition results in excessive elongation of the hypocotyl
336 under WLFR, since PIF7 action is no longer constrained by phyA.

337 The movement of phyA to the nucleus in WLFR is strongly contingent on the chaperone
338 proteins FHY1 and FHL7. Through the use of BiFc, split nanoLUC and co-
339 immunoprecipitation assays, we demonstrated that PIF7 also interacts with FHY1 and FHL
340 under WLFR. Fluorescent tagged versions of PIF7, phyA and FHY1/FHL illustrated that these
341 proteins co-localize within nuclei, suggesting the formation of PIF7-phyA-FHY1/FHL
342 complexes. Nuclear shuttling of phyA is a highly dynamic process that operates continuously
343 under WLFR conditions[9,37]. Earlier work indicates that dissociation of the phyA-FHY1/FHL
344 complex is required to both recycle the shuttle proteins and to facilitate phyA signaling[31,37]. We
345 therefore propose that PIF7 may serve to trap phyA and FHY1/FHL in inactive complexes,
346 which simultaneously perturbs the nuclear transport of phyA and disconnects it from
347 downstream signaling. Consistent with this interpretation, we find *pif7-1* and PIF7ox have
348 higher proportions of nuclear, and cytosolic phyA, respectively (Fig. 4b-e). Further, our genetic
349 data shows that phyA-NLS, which is constitutively nuclear, and bypasses the FHY1/FHL
350 shuttling mechanism, can restore phyA function to PIF7ox in WLFR, in terms of hypocotyl
351 phenotype and *CHS* and *IAA29* gene expression (Fig. 6g, Fig. S5). We also discovered that PIF7
352 reduces the expression of *ARABIDOPSIS SUMO PROTEASE 1 (ASP1)*, which aids the
353 deSUMOylation of FHY1 under FR light, thereby preventing its degradation. *ASP1* suppression
354 may, therefore, represent an alternative mechanism through which PIF7 modulates phyA

shuttling. Previously, our research demonstrated that under simulated shade, PIF7 interacts with and suppresses the transcriptional activity of ANGUSTIFOLIA 3 (AN3), a promoter of leaf cell proliferation[38]. In this case, PIF7 operates by evicting and substituting for AN3 at target promoters. Thus, in shade conditions, PIF7 assembles different nuclear complexes which execute distinct functions.

In summary, our study outlines the central role PIF7 plays in regulating phyA activity. Its direct binding to phyA, and the FHY1/FHL chaperones, likely represents a rapid, energy-efficient, and highly effective way to stem phyA action. The compartmentalization of phyA and FHY1/FHL into PIF7 photobodies constitutes a dynamic regulatory mechanism that responds to changes in environmental light quality. This subcellular partitioning enables PIF7 to drive hypocotyl elongation while simultaneously reducing the suppressive influence of phyA. Since the modulation of PIF7 by phyB is well-established, our findings position PIF7 at the molecular intersection of phyB and phyA, underscoring its pivotal role in adjusting phyA activity to promote SAS elongation under vegetative shade[19].

METHODS

Plant material and growth conditions

The wild-type of *Arabidopsis thaliana* seedlings are Columbia-0 (Col-0). The *pif7-1*, *pif7-2*[39], *pif8-1*, *pif8-2* mutants, and the construction of *pif8-1;phyA-211*, PIF8ox*;phyA-211* and PIF8ox[15], PIF7ox-FLASH[40], *p35S::GFP-PIF7*[20], *p35S::PIF3-LUC*[41], *p35S::PIF5-HA*, *p35S::PIF4-LUC*[16], *pPHYA::PHYA-sGFP, pPHYA::PHYA-sGFP-NLS*[25], and *pPHYA::PHYA-nanoLUC-3×FLAG-10×His* (phyA-nLUC)[3] have been described previously. The *phyA-211* mutant was obtained from NASC collection. *pPIF7::PIF7-nanoLUC-3×FLAG-10×His* (PIF7-nLUC) (Basta) were transformed into the *pif7-1* background. The *pif7-1*;phyA-GFP-NLS, and PIF7ox;phyA-GFP-NLS, *pif7-1*;*phyA-211* and PIF7ox;*phyA-211* lines were generated by genetic crossing. Likewise, the *pif7-1;*phyA-nLUC, PIF7ox;phyA-nLUC, PIF7-nLUC; *phyA-211* lines were made through genetic crossing. All the cross lines were verified using PCR or sequencing.

382 For the hypocotyl growth experiments seeds were first sterilized and then re-suspended in 0.1%
383 (w/v) agar and stored in darkness at 4 °C for 3 d to stratify. Following this, seeds were
384 individually sown onto plates containing half-strength Murashige and Skoog basal salts mixture
385 (Duchefa Biochemie, Haarlem, Netherlands) dissolved in 1% (w/v) agar (1/2 MS media; pH
386 5.8). The plates were then transferred to Percival I30BLL growth chambers at 22 °C (Plant
387 Climatics, Wertingen, Germany). To promote germination seeds were exposed to a 4 h period
388 of white light (WL) (85±5 μmol m^{-2} s^{-1}), and then darkness for 20 h, before transferring to
389 experimental photoperiods. For all experiments, seedlings were grown under short day (8L:16D)
390 conditions in either WL or WL with supplementary FR (WLFR) to provide a R:FR ratio of 0.20,
391 PAR=85±5 μmol m^{-2} s^{-1}.

392 **RNA extraction and qPCR**

393 For RNA extraction seedlings (n = 36 ± 5 seedling numbers), were harvested at Zeitgeber time
394 7 (ZT), one hour before dusk. Total RNA was extracted using a phenol-based method[38], 300 μL
395 RNA extraction buffer (PH=8.0) was added to each sample, followed by 300 μL 1:1 acidic
396 phenol: chloroform. The supernatant was separated from the pellet by centrifuging for 15
397 minutes at 13,000 rpm under 4 ºC. Up to 300 μL of the supernatant was transferred to collection
398 tubes with 240 μL isopropanol and 30 μL 3 M sodium acetate. Samples were precipitated at -
399 80 ºC for 15 minutes, then centrifuged for 30 minutes at 13,000 rpm. Pellets were washed with
400 300 μL of 70% ethanol and then suspended in nuclease-free water and stored at -80 ºC .
401 Complementary DNA (cDNA) synthesis was performed using the qScript cDNA SuperMix
402 (Quanta Biosciences) as described by the manufacturer. A Lightcycler 480 system (Roche) was
403 employed for qPCR, with 10 μL reactions that incorporated the SYBR Green Master Mix
404 (Roche). The qPCR primers are shown in **Supplementary Table 2**. Results were analyzed
405 using Light Cycler 480 (Roche) followed by the ΔΔCt method.

406 **Hypocotyl measurements and statistical analysis**

407 Images of hypocotyls were taken after 6 days of growth. Hypocotyl length was analyzed using
408 ImageJ (https://imagej.nih.gov/ij/). Data were analyzed by Excel and GraphPad Prism 10. Data
409 are presented as mean values ± s.e.m. Two-way ANOVA (α=0.05) was conducted to assess
410 statistical significance across light conditions for each genotype; asterisks denote significance
411 relative to control treatments: 0.1234 (ns), 0.0332 (*), 0.0021 (**), 0.0002 (***), P < 0.0001
412 (****). Representative data from three independent replicates are shown.

413 **Construct assembly**

414 The full-length CDS of *PHYA* and nanoLUC tag (*nanoLUC-3×FLAG-10×His*; NL3F10H)
415 have been described previously[3]. The CDS of *PIF7* were synthesized by the GeneArt Gene
416 Synthesis service (Invitrogen, MA, USA). The split nanoLUC tags were made by splitting
417 nanoLUC to lgbit (158 aa) and smbit (11 aa). Mobius Assembly[42] was used to insert the
418 constructs into a mUAV plasmid (L0, CamR) with *AraI* restriction site and plasmid assembly
419 was performed and subsequently verified by the Edinburgh Genome Foundry. The full-length
420 CDS of *FHY1* and *FHL* parts were amplified with Q5 High-Fidelity DNA polymerase (New
421 England Biolabs, MA, USA) from the Col-0 genome by gene-specific primers. The *PHYA-C*,
422 *PHYA-C1*, *PHYA-P*, *PHYA-H*, *PIF7-N*, *PIF7-B* and *PIF7-C* part cloned on the CDS region of
423 *PHYA* and *PIF7* (L0 parts). These parts were assembled into a mUAV plasmid and sequenced
424 by Source Bioscience (Cambridge, UK). All L0 parts will assemble in pMAP B L1 (KamR)
425 vector with *BsaI* restriction site. All the constructs for the tobacco (*Nicotiana benthamiana*)
426 assay used a CaMV35S promoter, which is synthesized by the GeneArt Gene Synthesis service
427 (Invitrogen, MA, USA).

428 To construct *pEXP601-pPIF7::PIF7-nanoLUC-3×FLAG-10×His*, a 2740 bp genomic
429 fragment was generated, encompassing the PIF7 promoter region (1015 bp), 5'UTR (161 bp),
430 and 1564 bp ORF, excluding the stop codon of exon 6 of the AT5G61270.1 gene model. This
431 fragment was PCR-amplified using specific primers with Phusion High-Fidelity DNA
432 Polymerase (NEB, M0530S). The resulting amplicon was subsequently recombined into
433 pDONR221 using BP II clonase (Invitrogen, 12535029), and its sequence verified by Sanger
434 sequencing (Genepool, Edinburgh Genomics, Edinburgh, UK). The genomic regions were then
435 recombined into *pGWB601:nanoLUC-3×FLAG-10×Hiss* using LR Clonase (Invitrogen)[43]. The
436 final construct was transformed into Agrobacterium AGL1. Primers used for construct
437 assembly are listed in **Supplementary Table 1.**

438 **The Tobacco Transient Expression Assay**

439 For this assay, constructs were transferred into the Agrobacterium AGL1 strain and cultured at
440 28 ºC for two days, before infiltration into 4-week-old *Nicotiana benthamiana* leaves with P19.
441 The transient expression solution contained 10 mM MES buffer (pH 5.6), 10 mM $MgCl_2$ and
442 200 mM aceto-syringone. Following infiltration plants were grown for 3 days in short day
443 (8L:16D, at 22 ºC) conditions in either WL or WLFR to provide a R:FR ratio of 0.20. Samples
444 were analyzed at ZT7 on day 3.

445 **Confocal Imaging, Colocalization, and BiFC**

446 Images of GFP, YFP and RFP fluorescence were obtained with a Leica confocal micro-scope

447 (Leica SP8) using 488 nm and 552 nm lasers. For BiFC and co-localization assay all images
448 were taken at ZT7 on day 3 after WL/WLFR treatments. The co-localization signals were
449 analyzed by LAS X Office 1.4.7.2982 and plotted by GraphPad Prism 10. *pPHYA::PHYA-*
450 *sGFP(NLS)*, *pif7-1*;phyA-GFP, PIF7ox;phyA-GFP and *p35S::GFP-PIF7* transgenic lines
451 images were taken at ZT7 within 30 minutes after 6 days of WL/WLFR treatments. The Nuclear
452 and cytosolic signals were quantified from cells in the mid-hypocotyl region within a 20 × 1.36
453 objective lens. Nucleus and cytoplasmic signals were quantified using Image J, after eliminating
454 background interference. Nuclear/cytoplasmic ratios were calculated and plotted in GraphPad
455 Prism 10[26]. Imaging experiments were comprised of three biological replicates, with 6 seedlings
456 per replicate.

457 **Immunoblot Analysis and Co-immunoprecipitation Assays**

458 Each sample comprised 0.5-1 g of Arabidopsis seedling tissue, harvested on day 6 at ZT7.
459 Samples were added to lysis buffer (125 mM Tris-HCl (pH 7.5); 0.25mM EDTA (pH 7.5), 150
460 mM NaCl, 5% glycerol, 0.1% Triton X-100, 0.5% NP-40), which contained 1× Protease
461 inhibitor (Sigma-Aldrich, P9599) and 1× HALT-Phosphatase inhibitor (Thermo Scientific).
462 Samples were centrifuged at 12,000 rpm for 10 mins at 4 ºC and then transferred to lysate mix
463 with 1× SDS loading buffer (containing 0.1 M DTT) at a 1:1 volume ratio. Samples were
464 incubated at 80 ºC for 10 mins, followed by a centrifugation step, before western blotting.

465 For Co-immunoprecipitation, after lysis an aliquot of the total protein was saved as an input
466 sample. Then, other total protein extracts were incubated with Protein A/G beads (MCE
467 Magnetic Agarose) for 1 h at 4 °C to remove adventitious binding proteins. Then anti-
468 FLAG/His beads (Anti-FLAG M2 agarose gel Sigma-Aldrich, Cat.No. A2220; Anti-His
469 Magnetic Beads, Cat. 209, MCE) were added into treated protein extracts and kept overnight
470 at 4 ºC. The antibody/protein complex was washed with wash buffer (125 mM Tris-HCl [pH
471 7.5]; 0.25mM EDTA [pH 7.5], 150 mM NaCl, 5% glycerol, 0.1 % Triton X-100) 5 times. Then,
472 50 µL of 1× SDS loading buffer were added to each sample and incubated at 80 ºC for 8 mins.

473 To detect native phyA protein, an anti-Phytochrome A antibody (PHYTOAB, PHY1907) was
474 used at 1:1,000. To detect the PIF7ox-FLASH and *p35S::FHY1/FHL-nanoLUC × 3FLAG×*
475 *10His* an anti-FLAG M2 antibody (Sigma-Aldrich, F1804) was used at 1:2,000. To detect the
476 *p35S::PIF7-sfGFP* an anti-GFP anti-body (Roche, ab290) was used at 1:3,000. Anti-RPN6
477 antibody (Agrisera, AS121858) was used at 1:3,000 as internal control. Secondary antibodies
478 (1:3,000, anti-mouse IgG (cell signaling, 7076s); 1:4,000 Goat anti-rabbit-IgG (Abcam,
479 AB6013) were used for the ECL Prime Western Blotting System. The signals were detected by
480 Azure 300 Imager with ECL prime western blotting detection reagents (Cytiva, RPN2232).

481 **NanoLUC and split nanoLUC assays**

482 NanoLUC bioluminescence assays were conducted as previously described[3]. Single
483 Arabidopsis seedlings were grown in individual wells, within a 96-well plate, each containing
484 200 µl 1/2 MS media. Plates were sealed with cling film and placed under 8L:16D (WL) for 6
485 days. Before imaging, 50 µl of 1:50 water dilution of Nano-Glo buffer (Promega, Nano-
486 Glo®Luciferase Assay) was added to the seedlings in each well. Plates were sealed and moved
487 to experimental light conditions. Bioluminescence was recorded every hour (for 1.5 s) for
488 several days using the TriStar2 LB942 multimode microplate reader (Berthold Technologies,
489 Germany). In **Fig. 1g**, the data were analyzed by averaging individual seedling measurements
490 and then calculating the fold change relative to the ZT0 data for each biological replicate.
491 Subsequently, the results were plotted using GraphPad Prism 10. A total of 9 biological
492 replicates were conducted, with each replicate comprising at least 6 seedlings. The data was
493 analyzed by BioDare2 software[44], applying amp&baseline detrending and normalization steps,
494 before plotting in GraphPad Prism 10 (**Fig. S2**)

495 The split nanoLUC assay utilized the *N. benthamiana* transient expression system described
496 above. Following WL/WLFR treatments for 3 days, 1cm x 1cm leaf samples (n =12) were
497 transferred to 96 wells plates containing 100 µl diluted (1:50) Nano-Glo for imaging with a
498 plate reader. The data analyzed by Excel and GraphPad Prism 10. Experiments repeated at least
499 3 times.

500 **Chromatin Immunoprecipitation (ChIP)-qPCR**

501 We employed ChIP-qPCR methods described previously[45]. For each sample 0.5-1 g of tissue
502 was extracted from 6 day -old seedlings at ZT7. Cross-linking was induced with 1%
503 formaldehyde under vacuum infiltration for 15 mins (up to -70 kPa), then 2.5 ml of 2 M glycine
504 was added to quench crosslinking. DNA was fragmented into an average size of ~150 bp in
505 Diagenode BioRuptor Plus, (30 cycles of high power 30s ON / 30s OFF). Anti- PHYA antibody
506 (PHYTOAB, PHY1907,1:300) incubated with protein A/G beads (MCE Magnetic Agarose) in
507 4 ºC overnight. And the following day, samples were incubated with protein A/G bead/PHYA
508 antibody complex for 6 hours at 4 ºC. DNA was extracted using phenol/chloroform (1:1,
509 vol/vol). Protein enrichment at DNA regions was quantified using qPCR with the primers
510 detailed in **Supplementary Table 2.** Enrichment was determined by %Input method (%Input=2
511 ^ [CtInput-CtChIP] × IDF × 100%).

512 **Nuclear-Cytoplasmic Fractionation**

513 Nuclear fractionation was performed essentially as previously described with the following

514 modifications[46]. Briefly, 0.5-1 g of Arabidopsis seedlings ground into fine powder in liquid
515 nitrogen and then homogenized in double the volume of pre-cooled (4 °C) lysis buffer (20 mM
516 Tris-HCl, pH 7.4, 25% Glycerol, 20 mM KCl, 2 mM EDTA, 2.5 mM $MgCl_2$, 250 mM Sucrose
517 and 5 mM DTT, add 1× protease inhibitor cocktail (Roche) and 1× HALT-Phosphatase
518 inhibitor added in fresh). The sample was filtered twice through two layers of Mira cloth (Merck
519 Millipore). The flow-through was spun 10 min at 2000 g, 4 °C. Supernatant, consisting of the
520 cytoplasmic fraction, was centrifuged 20 min at 13,000 g, 4 °C and collected. The pellet,
521 containing the nuclear fraction, was washed six times with 2.5 mL of nuclear resuspension
522 buffer NRBT1 (20 mM Tris-HCl, pH 7.4, 25% Glycerol, 2.5 mM $MgCl_2$, 0.2% Triton X-100)
523 and centrifuged 3 min at 1,500 g, 4 °C. The pellet was resuspended in 300 µL of pre-cooled
524 NRBT2 (250 mM Sucrose, 10 mM Tris-HCl, pH 7.5, 10 mM $MgCl_2$, 1% Triton X-100, 0.035%
525 β-mercaptoethanol, and 1× protease inhibitor cocktail added in fresh), and carefully overlaid
526 on top of 300 µL NRBT3(1.7 M Sucrose, 10 mM Tris-HCl, pH 7.5, 2 mM $MgCl_2$, 0.15% Triton
527 X-100, 0.035% β-mercaptoethanol, and 1× protease inhibitor cocktail added in fresh). These
528 were centrifuged at 16,000 g for 55 min at 4 °C, and the final nuclear pellet was resuspended
529 in 2× SDS loading buffer. As quality controls for the fractionation, RbCL (Agrisera, AS03037,
530 1:3,000) protein was used as the cytoplasmic control, and histone H3 (Abcam, ab18521, 1:3,000)
531 was used as the nuclear control in immunoblot assays.

532 **ACKNOWLEDGEMENTS**

533 This research was supported by University of Edinburgh Darwin Trust Scholarship awarded to
534 MK. Z and Leverhulme Trust grant RPG-2024-082 awarded to K.J.H. We thank Dr. Rist Van
535 de Weyer who generated PIF7ox;*phyA-211* and first observed the PIF7ox hypocotyl phenotype
536 in WLFR. We thank Prof. Lin Li, Prof. Dr. Andreas Hiltbrunner and Dr. Gabriela Toledo-Ortiz
537 who kindly shared *p35S::GFP-PIF7*, *p35S::PHYA-RFP* and *pPHYA::PHYA-sGFP*(NLS) seeds
538 and thank Prof. Giltsu Choi for sharing *pif8-1;phyA-211*, *PIF8ox;phyA-211* and PIF8ox lines.

539 **AUTHOR CONTRIBUTIONS**

540 MK.Z and K.J.H. planned and designed the research. MK.Z conducted the experiments, which
541 were analyzed by K.J.H. and MK.Z. A.R. generated the *pPIF7::PIF7-nanoLUC* line. The
542 manuscript was prepared by MK.Z and K.J.H, subsequent editing performed by K.J.H and A.R.

543 **REFERENCES**

544 1 Liu, Y., Jafari, F. & Wang, H. Y. Integration of light and hormone signaling pathways in
545 the regulation of plant shade avoidance syndrome. *Abiotech* **2**, 131-145 (2021).
546 https://doi.org:10.1007/s42994-021-00038-1.

2 Franklin, K. A. Shade avoidance. *New Phytol* **179**, 930-944 (2008). https://doi.org:10.1111/j.1469-8137.2008.02507.x.

3 Butlin, P., Valdivia-Cabrera, M., Grima, R. & Halliday, K. J. Arabidopsis thaliana Phytochrome A Sensory Properties in Canopy Shade. *bioRxiv* (2025). https://doi.org:10.1101/2025.05.14.654025.

4 Mathews, S. & Sharrock, R. A. Phytochrome gene diversity. *Plant Cell Environ* **20**, 666-671 (1997). https://doi.org:10.1046/j.1365-3040.1997.d01-117.x.

5 Cheng, M. C., Kathare, P. K., Paik, I. & Huq, E. Phytochrome Signaling Networks. *Annu Rev Plant Biol* **72**, 217-244 (2021). https://doi.org:10.1146/annurev-arplant-080620-024221.

6 Du, J., Kim, K. & Chen, M. Distinguishing individual photobodies using Oligopaints reveals thermo-sensitive and -insensitive phytochrome B condensation at distinct subnuclear locations. *Nature Communications* **15** (2024). https://doi.org:10.1038/s41467-024-47789-1.

7 Casal, J. J., Luccioni, L. G., Oliverio, K. A. & Boccalandro, H. E. Light, phytochrome signalling and photomorphogenesis in. *Photoch Photobio Sci* **2**, 625-636 (2003).https://doi.org:10.1039/b300094j.

8 Rausenberger, J. *et al.* Photoconversion and Nuclear Trafficking Cycles Determine Phytochrome A's Response Profile to Far-Red Light. *Cell* **146**, 813-825 (2011). https://doi.org:10.1016/j.cell.2011.07.023.

9 Hiltbrunner, A. *et al.* Nuclear accumulation of the phytochrome A photoreceptor requires FHY1. *Curr Biol* **15**, 2125-2130 (2005). https://doi.org:10.1016/j.cub.2005.10.042.

10 Genoud, T. *et al.* FHY1 Mediates Nuclear Import of the Light-Activated Phytochrome A Photoreceptor. *Plos Genet* **4** (2008). https://doi.org:10.1371/journal.pgen.1000143.

11 Li, J. G. *et al.* Transcription Factor ELONGATED HYPOCOTYL5 Plays a Role in the Feedback Regulation of Phytochrome A Signaling. *Plant Cell* **22**, 3634-3649 (2010). https://doi.org:10.1105/tpc.110.075788.

12 Pham, V. N., Kathare, P. K. & Huq, E. Phytochromes and Phytochrome Interacting Factors. *Plant Physiol* **176**, 1025-1038 (2018). https://doi.org:10.1104/pp.17.01384.

13 Jeong, J., Lee, Y. & Choi, G. Both phytochrome A and phyB interact with PHYTOCHROME-INTERACTING FACTORs through an evolutionary conserved phy(OPM)-APA interaction. *Nat Commun* **16**, 3946 (2025). https://doi.org:10.1038/s41467-025-59327-8.

14 Al-Sady, B., Ni, W., Kircher, S., Schafer, E. & Quail, P. H. Photoactivated phytochrome induces rapid PIF3 phosphorylation prior to proteasome-mediated degradation. *Mol Cell* **23**, 439-446 (2006). https://doi.org:10.1016/j.molcel.2006.06.011.

15 Oh, J., Park, E., Song, K., Bae, G. & Choi, G. PHYTOCHROME INTERACTING FACTOR8 Inhibits Phytochrome A-Mediated Far-Red Light Responses in Arabidopsis. *Plant Cell* **32**, 186-205 (2020). https://doi.org:10.1105/tpc.19.00515.

16 Seaton, D. D. *et al.* Dawn and photoperiod sensing by phytochrome A. *P Natl Acad Sci USA* **115**, 10523-10528 (2018). https://doi.org:10.1073/pnas.1803398115.

17 Zhu, T., Yang, C., Xie, Y., Huang, S. & Li, L. Shade-induced lncRNA PUAR promotes shade response by repressing PHYA expression. *EMBO Rep* **24**, e56105 (2023). https://doi.org:10.15252/embr.202256105.

18 Leivar, P. *et al.* The Arabidopsis phytochrome-interacting factor PIF7, together with PIF3 and PIF4, regulates responses to prolonged red light by modulating phyB levels. *Plant Cell* **20**, 337-352 (2008). https://doi.org:10.1105/tpc.107.052142.

19 Xie, Y. *et al.* Phytochrome B inhibits the activity of phytochrome-interacting factor 7 involving phase separation. *Cell Rep* **42** (2023). https://doi.org:10.1016/j.celrep.2023.113562.

20 Huang, X. *et al.* Shade-induced nuclear localization of PIF7 is regulated by phosphorylation and 14-3-3 proteins in Arabidopsis. *Elife* **7** (2018). https://doi.org:10.7554/eLife.31636.

21 Park, E. *et al.* Phytochrome B inhibits binding of phytochrome-interacting factors to their target promoters. *Plant Journal* **72**, 537-546 (2012). https://doi.org:10.1111/j.1365-313X.2012.05114.x.

22 Ni, M., Tepperman, J. M. & Quail, P. H. PIF3, a phytochrome-interacting factor necessary for normal photoinduced signal transduction, is a novel basic helix-loop-helix protein. Cell 95, 657-667 (1998). https://doi.org:10.1016/S0092-8674(00)81636-0.

23 Lorrain, S., Trevisan, M., Pradervand, S. & Fankhauser, C. Phytochrome interacting factors 4 and 5 redundantly limit seedling de-etiolation in continuous far-red light. *Plant Journal* **60**, 449-461 (2009). https://doi.org:10.1111/j.1365-313X.2009.03971.x.

24 Kevei, E., Schafer, E. & Nagy, F. Light-regulated nucleo-cytoplasmic partitioning of phytochromes. *J Exp Bot* **58**, 3113-3124 (2007). https://doi.org:10.1093/jxb/erm145.

25 Toledo-Ortiz, G. *et al.* Subcellular sites of the signal transduction and degradation of phytochrome A. *Plant Cell Physiol* **51**, 1648-1660 (2010). https://doi.org:10.1093/pcp/pcq121.

26 Chen, F. *et al.* Phosphorylation of FAR-RED ELONGATED HYPOCOTYL1 is a key mechanism defining signaling dynamics of phytochrome A under red and far-red light in Arabidopsis. *Plant Cell* **24**, 1907-1920 (2012). https://doi.org:10.1105/tpc.112.097733.

27 Wang, H. & Deng, X. W. Arabidopsis FHY3 defines a key phytochrome A signaling component directly interacting with its homologous partner FAR1. *EMBO J* **21**, 1339-1349 (2002). https://doi.org:10.1093/emboj/21.6.1339.

28 Qu, G. P. *et al.* Reversible SUMOylation of FHY1 Regulates Phytochrome A Signaling in Arabidopsis. *Mol Plant* **13**, 879-893 (2020). https://doi.org:10.1016/j.molp.2020.04.002.

29 Toledo-Ortiz, G. *et al.* Subcellular sites of the signal transduction and degradation of phytochrome A. *Plant Cell Physiol* **51**, 1648-1660 (2010). https://doi.org:10.1093/pcp/pcq121.

30 Menon, C., Klose, C. & Hiltbrunner, A. Arabidopsis FHY1 and FHY1-LIKE Are Not Required for Phytochrome A Signal Transduction in the Nucleus. *Plant Commun* **1**, 100007 (2020). https://doi.org:10.1016/j.xplc.2019.100007.

31 Rausenberger, J. *et al.* Photoconversion and Nuclear Trafficking Cycles Determine Phytochrome A's Response Profile to Far-Red Light. *Cell* **146**, 813-825 (2011). https://doi.org:10.1016/j.cell.2011.07.023.

32 Al-Sady, B., Ni, W., Kircher, S., Schafer, E. & Quail, P. H. Photoactivated phytochrome induces rapid PIF3 phosphorylation prior to proteasome-mediated degradation. *Mol Cell* **23**, 439-446 (2006). https://doi.org:10.1016/j.molcel.2006.06.011.

33 Shen, H. *et al.* Light-induced phosphorylation and degradation of the negative regulator

PHYTOCHROME-INTERACTING FACTOR1 from depend upon its direct physical interactions with photoactivated phytochromes. *Plant Cell* **20**, 1586-1602 (2008). https://doi.org:10.1105/tpc.108.060020.

34 Kim, C. *et al.* Phytochrome B photobodies are comprised of phytochrome B and its primary and secondary interacting proteins. *Nature Communications* **14** (2023). https://doi.org:10.1038/s41467-023-37421-z.

35 Zhang, X. Y. *et al.* Liquid-liquid phase separation in diseases. *Medcomm* **5** (2024). https://doi.org:e64010.1002/mco2.640.

36 Chen, D. *et al.* Integration of light and temperature sensing by liquid-liquid phase separation of phytochrome B. *Mol Cell* **82**, 3015-+ (2022). https://doi.org:10.1016/j.molcel.2022.05.026.

37 Genoud, T. et al. FHY1 Mediates Nuclear Import of the Light-Activated Phytochrome A Photoreceptor. Plos Genet 4 (2008). https://doi.org:100014310.1371/journal.pgen.1000143.

38 Hussain, E., Romanowski, A. & Halliday, K. J. PIF7 controls leaf cell proliferation through an AN3 substitution repression mechanism. *P Natl Acad Sci USA* **119** (2022). https://doi.org:10.1073/pnas.2115682119.

39 Leivar, P. *et al.* Multiple Phytochrome-Interacting bHLH Transcription Factors Repress Premature Seedling Photomorphogenesis in Darkness. *Curr Biol* **18**, 1815-1823 (2008). https://doi.org:10.1016/j.cub.2008.10.058.

40 Li, L. *et al.* Linking photoreceptor excitation to changes in plant architecture. *Genes Dev* **26**, 785-790 (2012). https://doi.org:10.1101/gad.187849.112.

41 Viczián, A. *et al.* Functional characterization of phytochrome interacting factor 3 for the circadian clockwork. *Plant and Cell Physiology* **46**, 1591-1602 (2005). https://doi.org:10.1093/pcp/pci175.

42 Andreou, A. I. & Nakayama, N. Mobius Assembly: A versatile Golden-Gate framework towards universal DNA assembly. Plos One 13 (2018). https://doi.org:10.1371/journal.pone.0189892.

43 Urquiza-García, U. & Millar, A. J. Expanding the bioluminescent reporter toolkit for plant science with NanoLUC. Plant Methods 15 (2019). https://doi.org:10.1186/s13007-019-0454-4.

44 Zielinski, T., Moore, A. M., Troup, E., Halliday, K. J. & Millar, A. J. Strengths and Limitations of Period Estimation Methods for Circadian Data. *Plos One* **9** (2014). https://doi.org:10.1371/journal.pone.0096462

45 Wang, Z. S. *et al.* Proteasome-associated ubiquitin ligase relays target plant hormone-specific transcriptional activators. *Sci Adv* **8** (2022). https://doi.org:10.1126/sciadv.abn4466.

46 Zhu, D. M. *et al.* Biochemical Characterization of Complexes Containing CONSTITUTIVELY PHOTOMORPHOGENIC1 and SUPPRESSOR OF PHYA Proteins in Light Control of Plant Development. *Plant Cell* **20**, 2307-2323 (2008). https://doi.org:10.1105/tpc.107.056580.

47 Rosler, J., Klein, I. & Zeidler, M. double mutant reveals a distinct cytoplasmic action of phytochrome A. *P Natl Acad Sci USA* **104**, 10737-10742 (2007). https://doi.org:10.1073/pnas.0703855104.

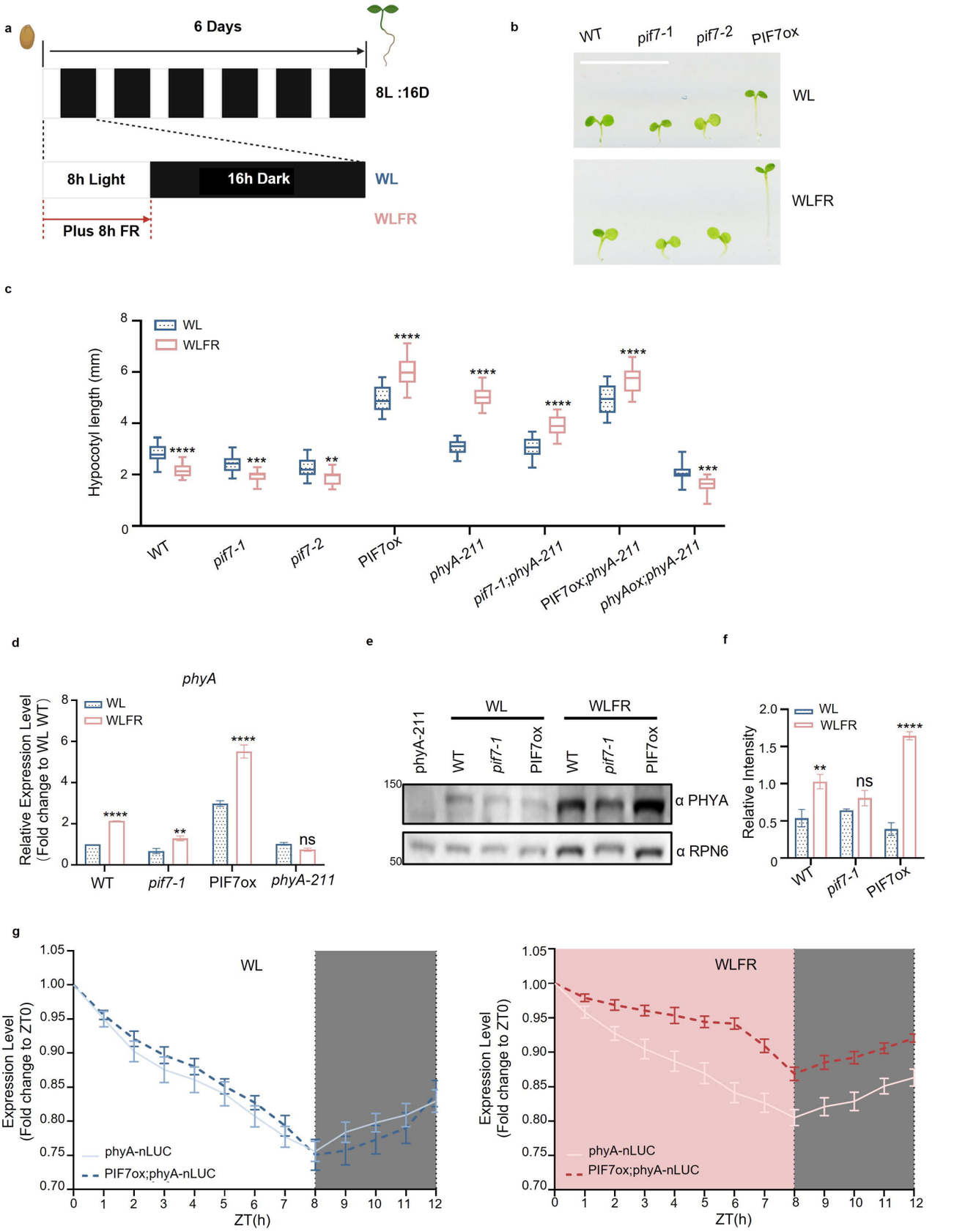

Fig. 1 PIF7ox influences phyA Function in WLFR

a, Schematic of experimental growth conditions. Seeds were sown on 1/2 MS plates and cultivated for one day under white light, followed by 4 hours (h) of light and 20 h of dark. Seedlings were subsequently grown for 6 days in white light (WL) photoperiods with or without supplementary far-red (WLFR), lowering the R:FR to 0.20 (red arrow). For all experiments, light regimes were 8 h light at PAR = 85 ± 5 μmol m^{-2} s^{-1}, 16 h dark, at 22°C.

b, Representative images of *Arabidopsis thaliana* WT (*Col-0*), *pif7-1*, *pif7-2*, and PIF7ox seedlings grown in WL or WLFR for 6 days. Scale bar = 1 cm.

c, PIF7ox blocks phyA action in WLFR. Hypocotyl length (mm) of WT (*Col-0*), *pif7-1*, *pif7-2*, PIF7ox, *phyA-211*, *pif7-1;phyA-211, PIF7ox;phyA-211* and phyAox under WL and WLFR. Representative images from three independent replicates are shown.

d, In WLFR, PIF7 enhances *PHYA* expression at Zeitgeber time 7 (ZT). Real-time qPCR was used to quantify *PHYA* mRNA levels, with *PP2A* as internal control. Samples were collected at ZT7 (1 hour before dusk) from 6d-old seedlings grown in WL or WLFR.

e,**f**, In WLFR, PIF7 increases PHYA protein accumulation. PHYA protein levels were determined by immunoblotting. Anti-PHYA was used to detect native phyA, while anti-RPN6 served as an internal control. The bar chart (**f**) displays the relative levels of phyA, normalised to RPN6, based on data from four biological replicates collected at ZT7.

g, PIF7ox boosts PHYA protein levels in diel conditions. The phyA-nLUC line was generated by expressing (p*PHYA::PHYA-nLUC*) in *phyA-211*, while the PIF7ox;phyA-nLUC was generated by introgressing p*PHYA::PHYA-nLUC* into the PIF7ox line. Bioluminescence signals were recorded from day 6.

For **c**,**d**,**f**,**g**, data are presented as mean values ± s.e.m., *n*=25 (seedling numbers) in **c**; with *n*=3,4,9 (biological repeats) in **d**,**f**,**g**, respectively. For **c**,**d**,**f**, a Two-way ANOVA was conducted to assess statistical significance across light conditions for each genotype (α=0.05); asterisks denote significance relative to WL treatments: 0.1234 (ns), 0.0332 (*), 0.0021 (**), 0.0002 (***), $P < 0.0001$ (****).

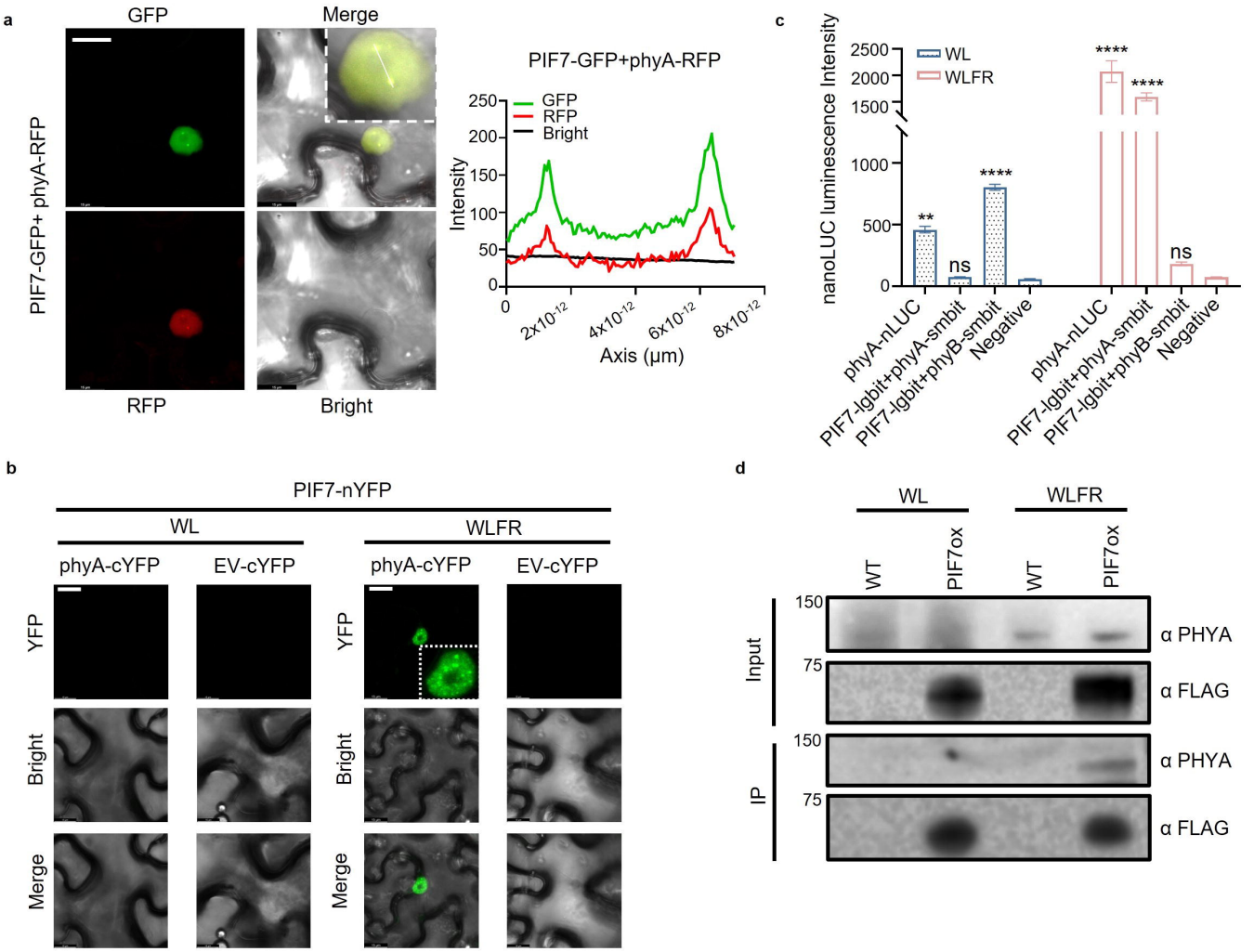

Fig. 2 PIF7 and phyA interact in sub-nuclear photobodies under WLFR.

a, *p35S::PIF7-sfGFP* and *p35S::PHYA-RFP* co-localise in nuclei and photobodies in WLFR. Co-localisation is evident from the chart (right) which traces the GFP and RFP channel signals along the white bar shown in merged nucleus image (left).

b, Bimolecular Fluorescence Complementation (BiFC) assay confirms PIF7 and phyA interact in nuclear photobodies. BiFC was detected between *p35S::PIF7-nYFP* and *p35S::PHYA*-cYFP (PIF7-nYFP + phyA-cYFP) in WLFR, but not with the *p35S::EV-cYFP* (EV-cYFP, empty vector) control.

c, Split NanoLUC (nLUC) assay demonstrates PIF7 and phyA physically interact. *p35S::*PIF7-lgbitnLUC (PIF7-lgbit), *p35S::PHYA-smbitnLUC* (phyA-smbit), *p35S::PHY*B-smbitnLUC (phyB-smbit) and *p35S::PHY*A-nLUC (phyA-nLUC) reporter constructs were expressed in *Nicotiana benthamiana*. A WLFR-dependent interaction was demonstrated for PIF7-lgbit+phyA-smbit. PhyA-nLUC was used as light conditional controls, and phyB-smbit+phyA-smbit as the negative control.

d, Co-immunoprecipitation assay (Co-IP) shows that phyA interacts with PIF7 in WLFR *in vivo*. Anti-His beads were used to pull down PIF7 from PIF7ox (*p35S::PIF7-FLASH*; 9×Myc-6×His-3×FLAG) or the WT(*Col-0*) negative control. Anti-PHYA and anti-FLAG used for detecting phyA and PIF7 respectively, in IP/Input. Samples were collected at ZT7 from 6-d old seedlings exposed to WL or WLFR.

For **a**,**b**, 488nm and 552nm laser detected the GFP/YFP and RFP signals. Scale Bar=15μm. For **c**, data are presented as mean values ± s.e.m., *n*=12 (leaf numbers). A Two-way ANOVA test was used to obtain statistical significance (α=0.05); asterisks denote statistical significance comparing negative to positive test or tested interaction treatments: 0.1234 (ns), 0.0332(*), 0.0021 (**), 0.0002(***), P<0.0001 (****). Representative images from three independent replicates are shown in all figs.

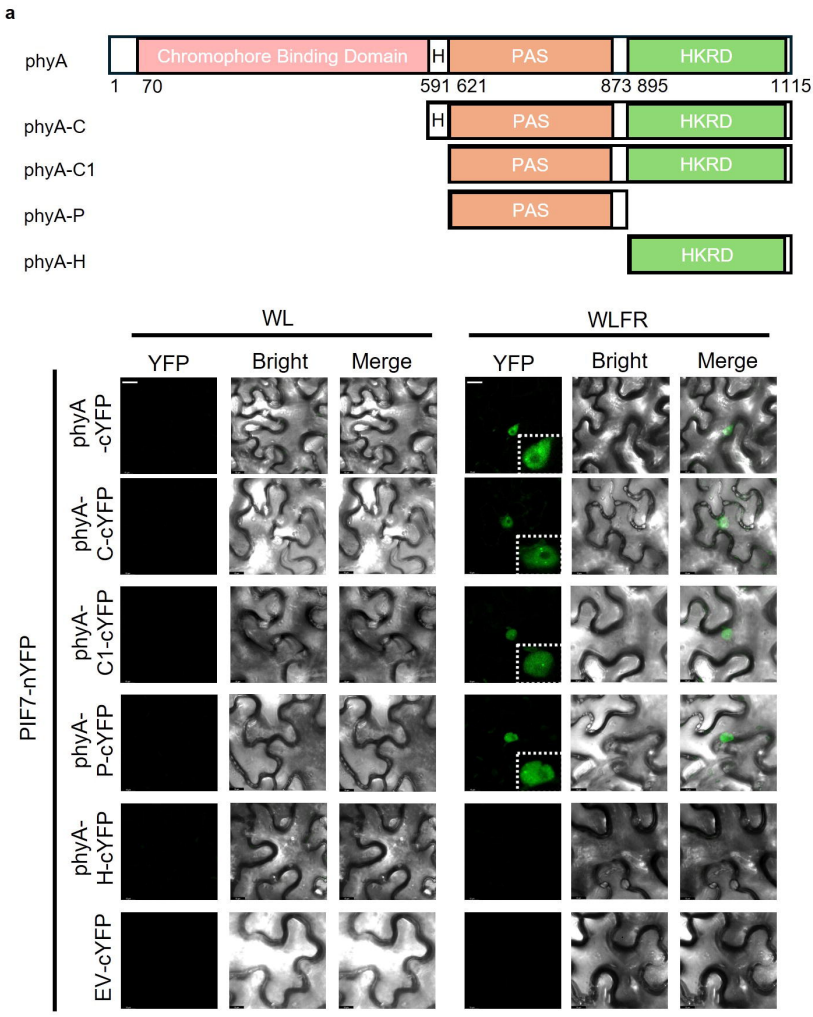

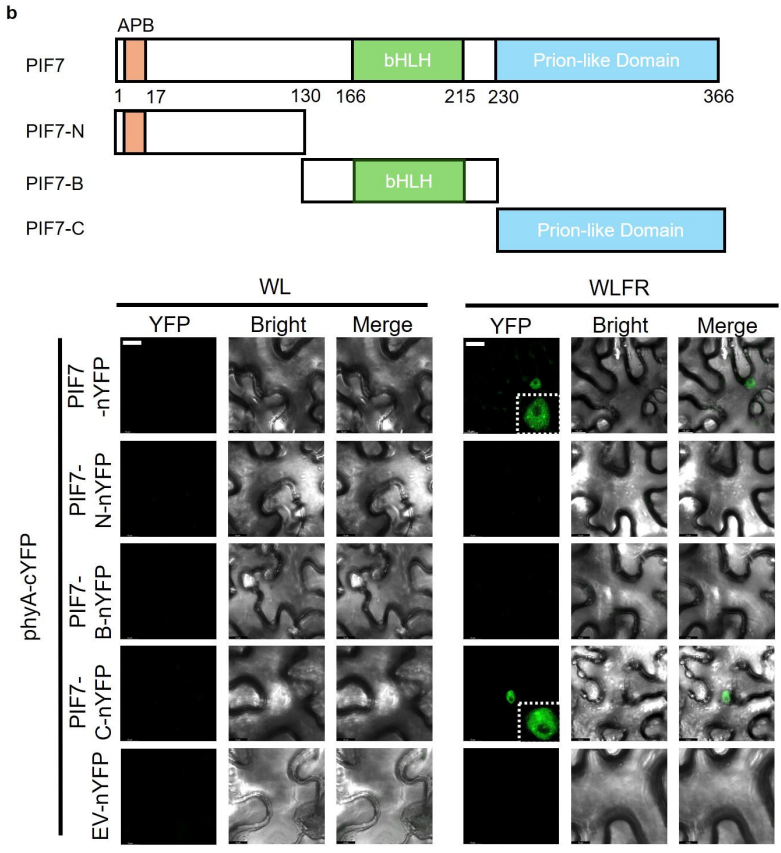

Fig. 3 The PIF7-phyA Interaction Depends on the PIF7 Prion like domain

a-b, BIFC assays using truncated constructs identify the PHYA PAS domain and the PIF7 prion-like domain, as important for the phyA-PIF7 interaction. The constructs image depicted the complete PHYA/PIF7 protein structures. Full length and truncated contructs were fused to C-terminal nYFP (PIF7) or cYFP (PHYA) BIFC constructs. PIF7-nYFP+phyA-cYFP was used as positive control and *p35S::EV-cYFP/p35S::EV-nYFP* (EV-cYFP/EV-nYFP) as used as negative controls. 488nm lasers were used to detect the YFP signals. Scale Bar=15μm. Representative images from three independent replicates are shown.

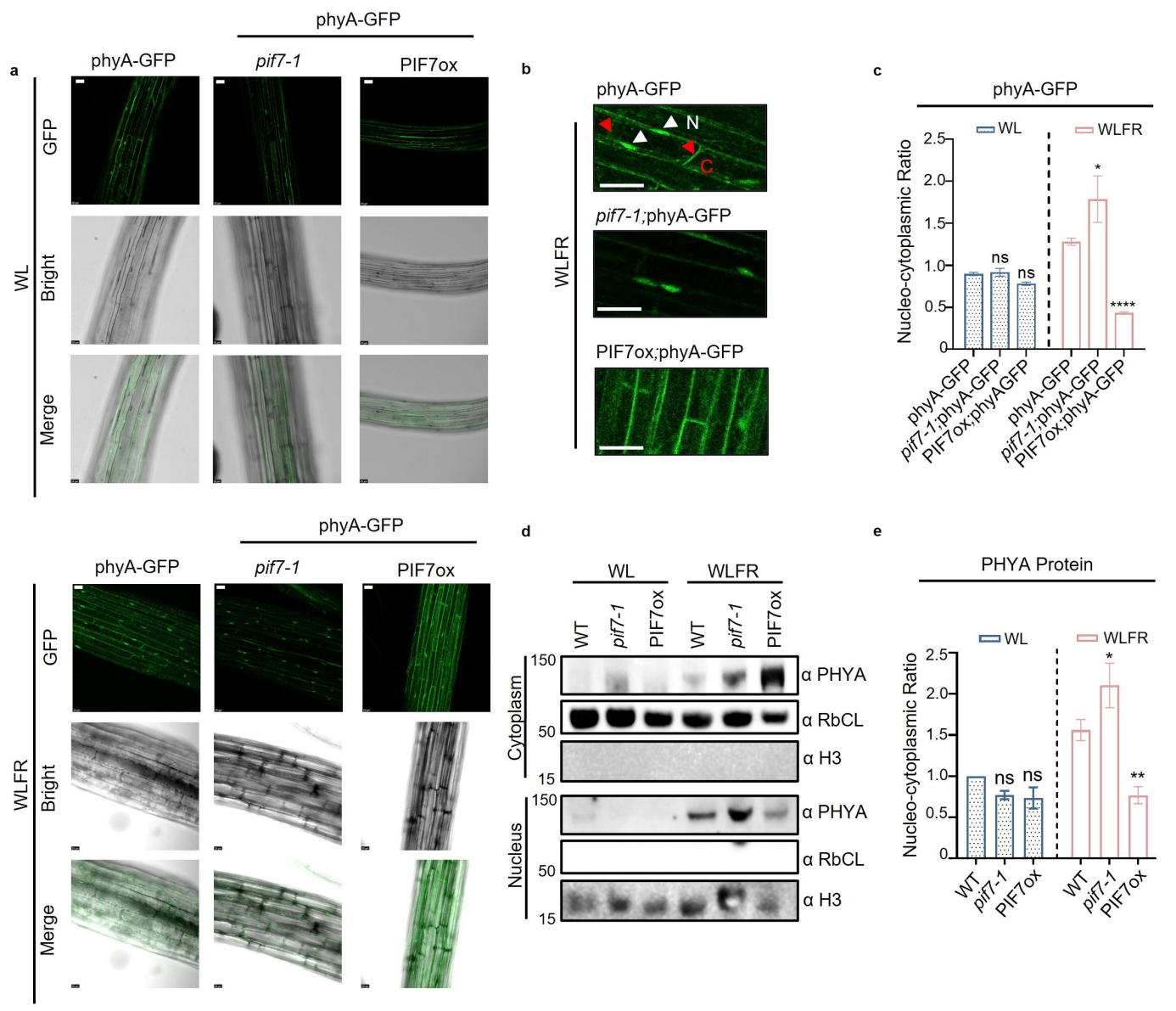

Fig. 4 PIF7 Influences the Sub-cellular Location of phyA

a-c, In WLFR, PIF7ox promotes accumulation of phyA-GFP in the cytosol. Lines of *pif7-1*;phyA-GFP and PIF7ox;phyA-GFP were generated by introgressing *pPHYA::PHYA-sGFP* into *pif7-1* and PIF7ox. Close-up images under WLFR are shown in **b**, white arrows and N label indicate nuclear, while red arrows and C label indicate cytosolic signals. In **c**, nuclear/cytosolic (N/C) ratios (relative to WT (*Col-0*), WL control) were calculated following quantification using ImageJ.

d-e, PIF7ox enhances PHYA protein accumulation in the cytosol under WLFR conditions. Immunoblot assays were conducted using an anti-PHYA antibody, using anti-RbCL as the cytosolic control, and anti-Histone 3 (H3) as the nuclear control. In **e**, cytoplasmic and nuclear phyA was normalised to RbCL and H3, respectively. The N/C ratio for each genotype is shown relative to WT (*Col-0*), WL control. Six-day-old seedlings were sampled as ZT7.

For **a-b** a wavelength of 488nm was used to detect GFP signals. Scale bar=25μm. Representative images from three independent replicates are shown. For **c**,**e**, data are presented as mean values ± s.e.m., n=6 (seedling numbers) in **c**; n=4 (biological repeats) in **e**. A two-way ANOVA test assessed statistical significance between genotypes under WL/WLFR condition (α=0.05); asterisks denote significance compared to the phyA-GFP (phyA N/C) values for WL/WLFR condition(**c**) or phyA protein (phyA N/C) values in WT with WL/WLFR condition(**e**): 0.1234 (ns), 0.0332 (*), 0.0021 (**), 0.0002 (***), $P < 0.0001$ (****).

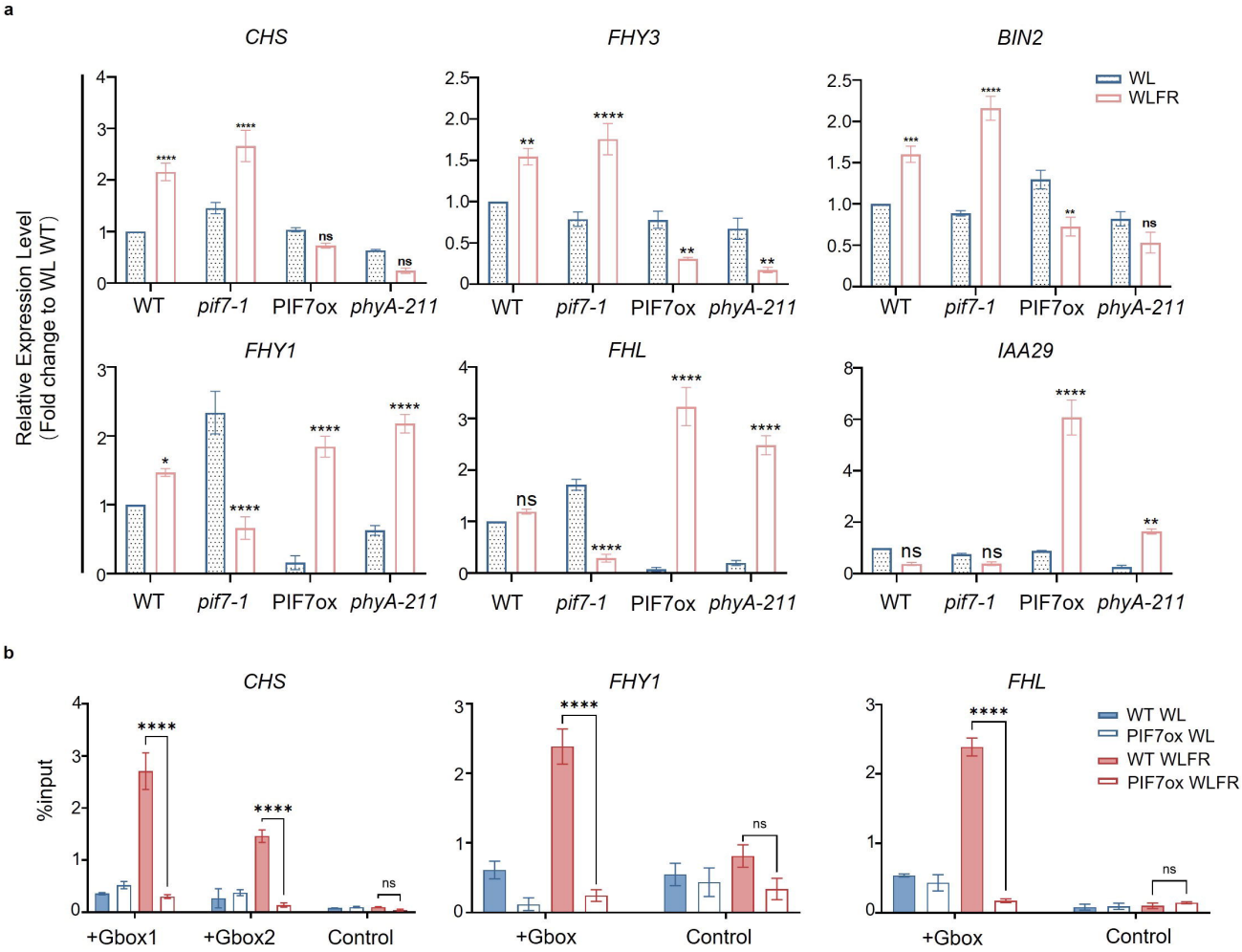

Fig. 5. PIF7 Inhibits phyA-Mediated Regulation of Target Genes

a, qPCR analysis of *CHS, FHY1, FHL, FHY3, BIN2,* and *IAA29* expression in WT (*Col-0*), *pif7-1*, PIF7ox and *phyA-211*. Transcript levels were normalised to the *PP2A* internal control.

b, PIF7ox reduces phyA enrichment at *CHS, FHY1,* and *FHL* promoters under WLFR. Chromatin immunoprecipitation (ChIP)-qPCR was conducted with 6-day-old WT (*Col-0*) or PIF7ox seedlings sampled at ZT7. Native phyA was immobilised on protein A/G beads using an anti-phyA antibody, and promoter enrichment quantified by qPCR at Gbox promoter regions and coding regions, which served as negative controls. Data shown is normalised to input samples.

For **a**-**b**, data are presented as mean values ± s.e.m., n=3 (biological repeats). A two-way ANOVA test was used to assess statistical significance between the WL/WLFR for each genotype (**a**) or different genotypes under the same conditions (**b**) (α=0.05); asterisks indicate statistical significance compared to control: 0.1234 (ns), 0.0332 (*), 0.0021 (**), 0.0002 (***), $P < 0.0001$ (****).

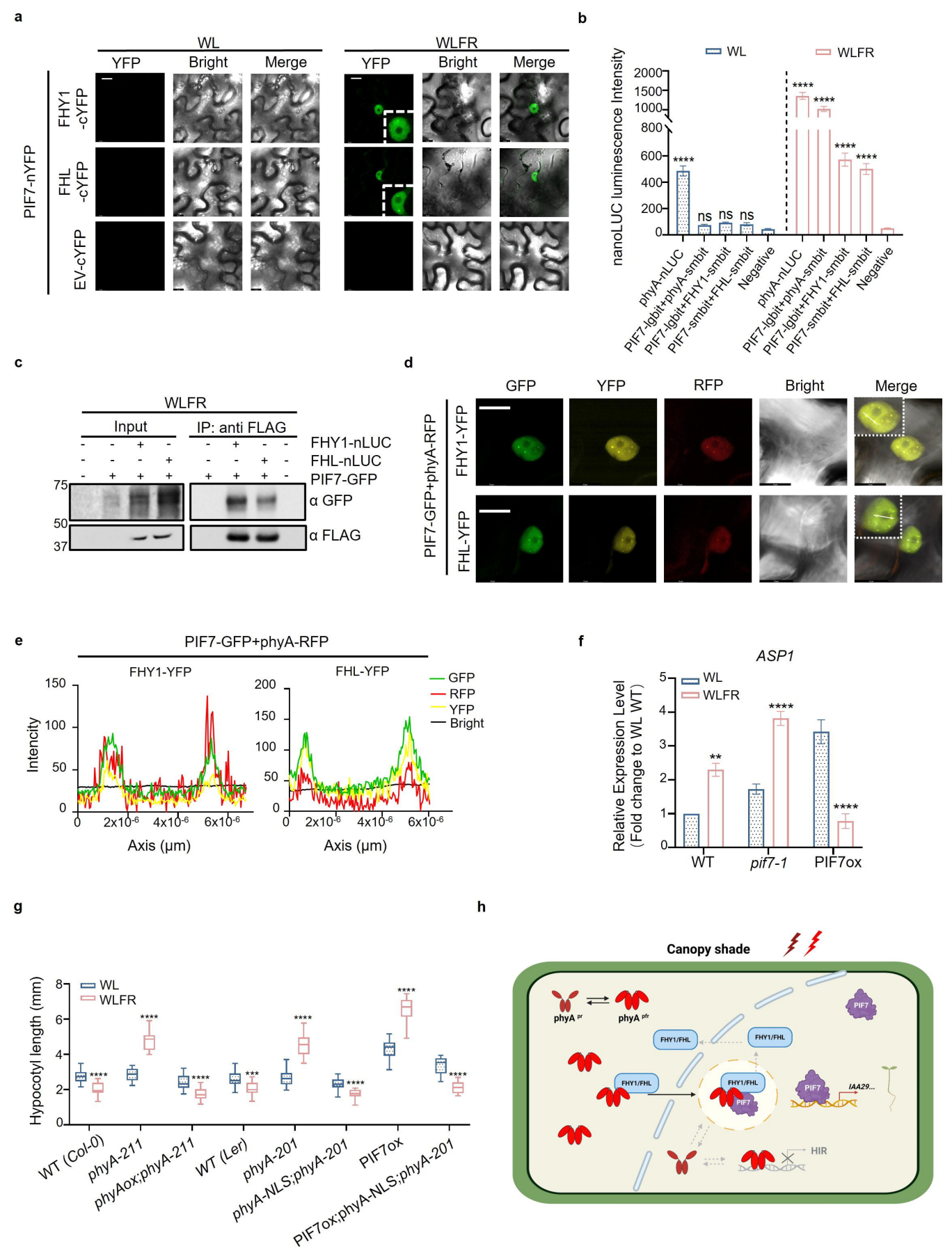

Fig. 6. PIF7 interacts with FHY1/FHL in WLFR

a, The BiFC assay demonstrates PIF7 interaction with FHY1 and FHL. Interaction fluorescence was detected when *p35S::FHY1-cYFP* (FHY1-cYFP) or *p35S::FHL-cYFP* (FHL-cYFP) were with expressed *p35S::PIF7-nYFP* (PIF7-nYFP) in *N. benthamiana* under WLFR.

b, Interactions between PIF7 and FHY1/FHL are detected using a split NanoLUC assay. Strong fluorescence signals were detected between *p35S::FHY1-smbitnLUC* (FHY1-smbit), *p35S::FHL-lgbitnLUC* (FHL-lgbit) and *p35S::PIF7-lgbit(smbit)nLUC* (PIF7-lgbit/smbit) in the transient *N. benthamiana* expression system. The positive controls were phyA-nLUC and PIF7-lgbit+phyA-smbit, while PIF7-smbit+phy-Asmbit was used as a negative control.

c, An immunoprecipitation assay demonstrates PIF7 interacts with FHY1/FHL *in vivo*. *p35S::FHY1/FHL-nanoLUC × 3FLAG× 10His* and *p35S::PIF7-sfGFP* constructs were transiently expressed in *N. benthamiana* leaves. Anti FLAG beads were used to pull down FHY1/FHL and its target proteins by Co-IP. Anti GFP antibodies revealed GFP-tagged PIF7 co-IP with FHY1/FHL in WLFR.

d-e, Fluorescence assays illustrate that PIF7, phyA and FHY1/FHL co-localise in nuclei and photobodies. *p35S::PIF7-sfGFP*, *p35S::FHY1/FHL-EYFP*, and *p35S::PHYA-RFP* constructs were transiently expressed in *N. benthamiana* leaves. The merged image (**d**) signifies co-localisation, and **e**, displays GFP, YFP and RFP channel signals relative to white bar shown in the merged nuclear image.

f, PIF7 reduces *ASP1* mRNA levels under WLFR. qPCR analysis of *ASP1* expression in WT, *pif7-1*, PIF7ox, *PP2A* was used as internal control.

g, phyA-NLS is epistatic to PIF7ox. Hypocotyl length (mm) is shown for WT (Col-0), *phyA-211, phyAox;phyA-211,* WT (Ler), *phyA-201, phyA-NLS;phyA-201*, *PIF7ox;phyA-NLS;phyA-201.* Double and triple mutant lines were generated through genetic.

h, Schematic depicting the cellular model for PIF7 control of phyA action in canopy shade. In WLFR PIF7 accumulates in the nucleus, where it interacts with phyA and FHL/FHY1 in photobodies. This sequestration not only blocks phyA from regulating downstream genes but also inhibits its transport into the nucleus. Consequently, PIF7 is able to amplify SAS-mediated hypocotyl elongation by blocking the antagonistic action of phyA. The image created in BioRender (https://BioRender.com).

For **a**,**d**, 488nm and 552nm lasers were used for detecting GFP/YFP and RFP signals. Scale bar=15μm. For **b**,**f**,**g**, data are presented as mean values ± s.e.m., *n*=12 (leaf numbers) in **b**; *n*=3 (biological repeats) in **f**; *n*=24 (seedling numbers) in **g**. A two-way ANOVA test was conducted to determine statistical significance (α=0.05), asterisks denote significance when comparing negative to positive controls and tested interactions (**b**) or compared to WL treatments in each genotype (**f-g**): 0.1234 (ns), 0.0332 (*), 0.0021 (**), 0.0002 (***), $P < 0.0001$ (****).